SPANDIDOS PUBLICATIONS

ONCOLOGY LETTERS 28: 381, 2024

Profilin 2 isoform expression is associated with lung metastasis of colorectal cancer according to a comprehensive gene expression study using a mouse model

NAOYUKI TOYOTA[1,2], MASASHI TSURUTA[1,3], YUKI TAJIMA[4], KOHEI SHIGETA[1], KOJI OKABAYASHI[1], HIROTOSHI HASEGAWA[5], SHIN FUJITA[2], YUKI YOSHIMATSU[6], IWAO OZAWA[6,7], TADASHI KONDO[7] and YUKO KITAGAWA[1]

[1]Department of Surgery, Keio University School of Medicine, Tokyo 160-8582, Japan; [2]Department of Colorectal Surgery, Tochigi Cancer Center, Utsunomiya, Tochigi 320-0834, Japan; [3]Department of Hepato-Biliary-Pancreatic and Gastrointestinal Surgery and Welfare, School of Medicine, International University of Health, Narita, Chiba 286-8520, Japan; [4]Department of Surgery, Hiratsuka City Hospital, Hiratsuka, Kanagawa 254-0065, Japan; [5]Department of Surgery, Tokyo Dental College Ichikawa General Hospital, Ichikawa, Chiba 272-8513, Japan; [6]Department of Patient-Derived Cancer Model, Tochigi Cancer Center, Utsunomiya, Tochigi 320-0834, Japan; [7]Department of Cancer Proteogenomics, Tochigi Cancer Center, Utsunomiya, Tochigi 320-0834, Japan

Received January 23, 2024; Accepted May 30, 2024

DOI: 10.3892/ol.2024.14514

Abstract. Lung metastasis is the second most common type of metastasis in colorectal cancer. Specific treatments for lung metastasis have not been developed since the underlying mechanisms are poorly understood. The present study aimed to elucidate the molecular basis of lung metastasis in colorectal cancer. In a mouse model, cell lines that were highly metastatic to the lungs were established by injecting colorectal cancer cells through the tail vein and removing them from the lungs. Differential gene expression comparing the transfected cells with their parental cells was investigated using DNA microarrays. The results were functionally interpreted using gene enrichment analysis and validated using reverse transcription-quantitative PCR (RT-qPCR). The isoforms of the identified genes were examined by melting curve analysis. The present study established colorectal cancer cell lines that were highly metastatic to the lungs. DNA microarray experiments revealed that genes (N-cadherin, VE-cadherin, *Six4*, Akt and VCAM1) involved in motility, proliferation and adhesion were upregulated, and genes (*tissue inhibitor of metalloproteinase-3* and *PAX6*) with tumor-suppressive functions were downregulated in metastatic cells. *Profilin 2* (*PFN2*) expression was upregulated in multiple metastatic cell lines using RT-qPCR. Two *PFN2* isoforms were overexpressed in metastatic cells. *In vitro* and *in vivo* models were established and genes associated with lung metastasis were identified to overcome the heterogeneity of the disease. Overall, aberrant *PFN2* expression is unreported in lung metastasis in colorectal cancer. In the present study, two *PFN2* isoforms with differential tissue distribution were upregulated in metastatic cells, suggesting that they promote lung metastasis in colorectal cancer.

Correspondence to: Dr Masashi Tsuruta, Department of Surgery, Keio University School of Medicine, 35 Shinanomachi, Shinjuku, Tokyo 160-8582, Japan
E-mail: masashitsuruta@gmail.com

Abbreviations: CRC, colorectal cancer; CT, computed tomography; DAVID, Database for Annotation, Visualization and Integrated Discovery; HDAC1, histone deacetylase 1; PFN2, Profilin 2; RT-PCR, reverse transcription PCR; TIMP3, tissue inhibitor of metalloproteinase-3

Key words: colorectal cancer, lung metastasis, microarray, profilin 2, isoforms

Introduction

Colorectal cancer (CRC) is one of the most prevalent malignant cancers, with the third highest incidence and second highest mortality rates among all cancers worldwide (1). Surgical resection offers a potentially high probability of cure, with approximately 90% of the patients having early-stage primary CRC. However, many patients are diagnosed at advanced stages, resulting in lower cure rates (2). According to recent research, 20-34% of patients newly diagnosed with CRC already exhibit metastatic disease (3), and 50-60% of individuals initially diagnosed with localized CRC eventually develop metastases (4). In particular, the liver is the most prevalent site for CRC metastasis, and the lungs are the second most prevalent one, accounting for approximately 10-18% of rectal and 5-6% of colon cancers (5). Surgical resection and chemotherapy are currently used to treat metastatic CRC. However, the clinical outcomes of patients with distant metastases remain poor, and the survival rate of patients with metastatic CRC remains below 20% (6). Therefore, the development of novel treatments based on an understanding of the molecular mechanisms of CRC progression is required.

In previous studies on metastatic CRC, liver metastasis is well investigated from the viewpoint of pathophysiological and molecular aspects owing to its high probability. During the process, TNF-α and IL-1β upregulate the expression of E-selectin and other adhesion molecules on liver sinusoidal endothelial cells and enhance liver metastases; VEGF mediates the vascularization (7).

Compared to liver metastasis, lung metastasis is thought to occur through different mechanisms. Lymphatic vessels in the colon and systemic venous circulation play more significant roles than those in the liver. Furthermore, the lung microenvironment is considerably more enriched with several types of immune cells that reside in the airways and alveoli than in the liver stroma (8). *SMAD4*-deficient CRC cells in a mouse model secrete CCL15, which recruits CCR1+ tumor-associated neutrophils, resulting in lung metastasis (9). NDRG1 plays an important role in MORC2-mediated CRC cell migration and invasion in vitro and promotes lung metastasis of CRC cells *in vivo* (10). Lung metastases share clonality with primary tumors (including *KRAS*, *TP53*, and *APC* mutations) through extensive genomic profiling of clinical samples from three patients with CRC (8). An animal study shows that HDAC1 plays a key role in lung metastasis by inhibiting EMT (11). Microarray analysis using metastatic lung tissue from six patients shows that 42 genes are upregulated in lung metastasis compared to those in the original colon tumor (12). Although these studies may lead to novel treatments, there is no consensus on the mechanism of lung metastasis since the results are inconsistent. We suspect that the heterogeneity of the samples can lead to this problem because most previous studies used a small number of tumor tissues derived from patients with different treatment histories or genetic backgrounds. Therefore, a more precise analysis of the mechanisms underlying lung metastasis is required.

We aimed to elucidate the mechanisms underlying lung metastasis of colorectal cancer. We used *in vitro* models to overcome the heterogeneity of the clinical materials. It is possible to obtain more accurate insights into lung metastasis by utilizing the experimental animal models and cell lines that we previously established since the mice we used were genetically homogeneous and each cell line was a single population.

In this study, we compared the gene expression profiles of the original cell line and cell lines established from lung metastasis to reveal the molecular background of lung metastasis in CRC. We found a unique difference in profilin 2 isoforms between primary and metastatic lung CRC cells.

Materials and methods

Cell culture. The CMT93-PM cell line was established in a previous study (13). Briefly, CMT93 cells (CCL-223; ATCC, Manassas, VA, USA) were injected into the tail veins of six-week-old female C57BL/6 mice. Twenty-five mice were used for this experiment. Eight weeks after the tail vein injection, all mice were euthanized by inducing anesthesia with 4.0% isoflurane and maintaining it with 2.0% isoflurane. Once general anesthesia was achieved, they were quickly sacrificed by exsanguination. The lungs were extracted and lung metastatic tumors were visually identified. The tumor tissues were used for primary tissue culture as previously described (13). The tumor cells were cultured and maintained in Dulbecco's modified Eagle's medium (Sigma-Aldrich, St. Louis, MO, USA) supplemented with 10% fetal bovine serum (v/v), 10,000 units/ml penicillin, 10,000 μg/ml streptomycin, and 25 μg/ml Gibco amphotericin B (Thermo Fisher Scientific, Tokyo, Japan) at 37˚C with 5% CO_2. Four metastatic tumors were subjected to primary tissue culture. Tumor cells from one metastatic tumor grew spontaneously, and the cells underwent more than 20 passages over a period of three months. The cells were designated as CMT93-PM and used in this study. Moreover, we assigned CMT93-PM cell numbers 1, 2, 3, and 4 according to the order in which they were collected. All animals were housed in a controlled environment at the Keio University School of Medicine under standard temperature and light and dark cycles. All animal procedures were approved by the Laboratory Animal Care and Use Committee of Keio University School of Medicine (approval no. 15006).

Evaluating metastatic potentials of CMT93 and CMT93-PM. CMT93-PM and CMT93-PM1 cells were injected into the eight-week-old male mice via the tail vein, as described above. Twenty-nine mice were used for this experiment. The number of metastatic tumors in the lungs was evaluated using computed tomography (CT) Before euthanasia, pulmonary metastasis was assessed using an X-ray micro-CT system (R_mCT2; Rigaku, Tokyo, Japan) under mild inhalation anesthesia using isoflurane. Chest CT operational parameters were set at 90 kV and 160 μA to utilize a respiratory and cardiac reconstruction mode according to the instruction manual. The field of view was 24x24 mm with a pixel size of 50x50 m. The scanning duration was 4.5 min. The mice were positioned prone to scanning, and inhalation anesthesia comprising a mixture of isoflurane (Pfizer Japan, Tokyo, Japan) and oxygen was administered via a nasal cone. The concentration of isoflurane was maintained at 2.0% from induction to maintenance. The respiratory and cardiac reconstruction modes allow X-ray images to be exclusively captured during the diastolic phase of the heart within the end-expiratory period. Imaging was performed by simultaneously tracking the breathing and cardiac movements under radiographic guidance. Examination was performed twice-at the 8 and 12th week after injection- to confirm pulmonary metastases by comparing the metachronous images obtained. All mice were euthanized at 12 weeks by cervical dislocation under general anesthesia using 4.0% isoflurane for induction. After euthanasia, the lungs were extracted and fixed by injecting 4% paraformaldehyde (PFA) (1 ml) through the trachea. The lung tissues were then immersed in 4% PFA and stored at room 4˚C for 48 h to facilitate fixation. Subsequently, they were dehydrated in absolute ethanol at 25˚C. The tissues were embedded in paraffin, and the paraffin blocks were cut into 4-μm thick sections. These sections were stained with Mayer's hematoxylin solution for 15 min at 25˚C, followed by rinsing in tap water. Finally, staining was conducted with eosin Y ethanol solution for 1 min at 25˚C. Pathological evaluation of pulmonary metastases was also conducted using Evos FL Auto2 microscope (Invitrogen, Carlsbad, CA, USA).

RNA extraction and microarrays. Total RNAs were extracted from CMT93 and CMT93-PM1 cells using an RNeasy Mini Kit (Qiagen, Valencia, CA, USA). Gene expression profiles were obtained using the Affymetrix GeneChip Mouse430_2 array following the manufacturer's instructions. Briefly, the sense-strand cDNA was fragmented and labeled using the Affymetrix GeneChip WT Terminal Labeling Kit (Santa Clara, CA, USA) after generating single-stranded cDNA. Following hybridization, the GeneChip Fluidics Station 450 (Affymetrix) was used to wash the arrays and scanning was performed using a GeneChip Scanner 3000 7G (Affymetrix). The raw intensity data derived from the microarray images were pre-processed using Affymetrix Expression Console software (Affymetrix). Expression intensities were stored as cell intensity files and normalized using the robust multi-chip average method. Subsequently, these datasets were subjected to filtering, with genes displaying an absolute fold change ≥2 or ≤0.5 identified as exhibiting differential expression. Subsequently, we conducted Gene Ontology analysis using the Database for Annotation, Visualization, and Integrated Discovery (DAVID) tool, and plotted the enrichment scores for each cluster (14), which served as indicators of the biological significance of these clusters.

Evaluating PFN2 expression using real-time-polymerase chain reaction (RT-PCR) and melting curve analysis. To evaluate the expression pattern of *PFN2* in the cell lines, RT-PCR with high-resolution melting curve analysis was sequentially performed on an LC480 platform (Roche Applied Science, Mannheim, Germany) in a reaction mixture containing 5 μl of 2xTHUNDERBIRD™ Next SYBR® qPCR Mix, 1.2 μl of profilin2-specific primer (forward: 5'-GCC TATACGTTGATGGTGACTG-3', and reverse: 5'-ACA AAGACCAAGACTCTCCCG-3'), 1 μl of cDNA and 2.8 μl of DNase-free water in a total reaction volume of 10 μl per sample. *GAPDH* (Hs99999903_m1) purchased from Applied Biosystems (Foster City, CA, USA) was used as a control. Two micrograms of total tissue RNA were reverse transcribed to generate cDNA using the High Capacity RNA-to-cDNA Kit (Applied Biosystems, Foster City, California, United States). The reaction conditions involved enzyme activation at 95˚Cx30 sec, followed by 50 cycles of denaturation at 95˚Cx5 sec, 53˚Cx20 sec for annealing, and 60˚Cx30 sec for extension (15). To analyze the relative changes in the quantitative RT-PCR, we employed the 2(-ΔΔCt) method (16). Following these reactions, high-resolution melting curve analysis was conducted by heating the mixture from 60-99˚C using a ramping degree of 4.8˚C/sec.

Detecting profilin splice forms by RT-PCR/Sanger sequencing. Real time PCR was performed and analyzed following the previously described protocol (15,16). cDNA was generated as described above. Polymerase chain reaction amplification was performed using *profilin 2*-specific primers. The same 3' primer (5'-GAGTCAAGGTGGGGAGCCAAC3') and a unique internal 5' primer (PFN2A: 5'-TCAAGTATTTTGCCA TTGAGTATGCC3', PFN2B: 5'-CCTCTTCAGGTATAAAGC GAGTTC3') were used. The PCR products were confirmed by Sanger sequencing. The PCR products were purified using the ExoSAP-IT® Express PCR Product Clean-up (Affymetrix, Santa Clara, California, United States) as per the manufacturer's instructions. Sanger sequencing reactions were prepared using the BigDye™ Terminator version 3.1 kit (Applied Biosystems, Foster City, California, United States) as per the manufacturer's instructions. Briefly, the sequencing reaction consisted of 1.75 μl Sequencing Reaction Mix (BigDye™ Terminator v3.1), 1 μl Sequencing Buffer (BigDye™ Terminator v1.1), 4.75 μl nuclease-free water, 1 μl forward primer, 1 μl reverse primer and 1 μl PCR product. The sequencing reaction was subjected to the following cycling conditions in a 2720 Thermal Cycler (Applied Biosystems, Foster City, California, United States): one cycle at 96˚C for 1 min, and 25 cycles at 96˚C for 13 sec, 50˚C for 8 sec, and 60˚C for 4 min. Sequence reactions were cleaned up with the AxyPrep Mag DyeClean Kit (Axygen, Union City, CA, United States) as per the manufacturer's instructions. Sequence raw reads were loaded onto the Seq studio Genetic Analyzer (PE Applied Biosystems) with Tracking Dye, Hi-Di™ Formamide (PE Applied Biosystems, Fostercity CA, USA).

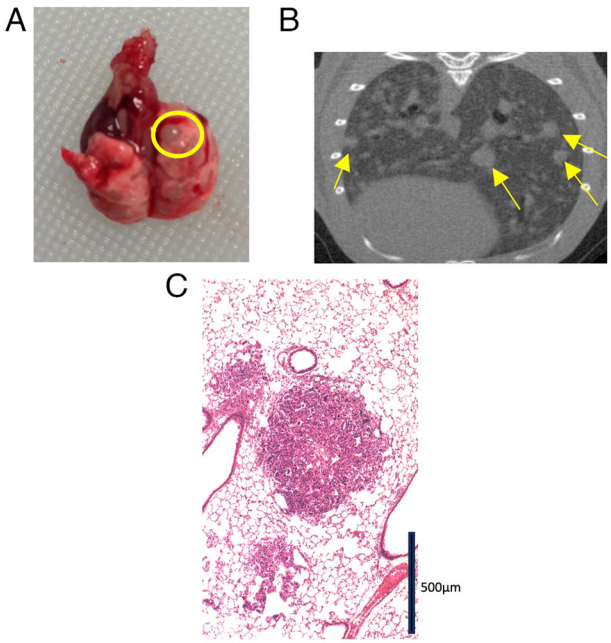

Figure 1. Metastatic function of CMT93-PM1. (A) Visual inspection of lung metastasis in CMT93 cells. The metastatic tumor is highlighted by a yellow circle. (B) Computed tomography images of multiple metastatic lung tumors of CMT93-PM1 cells. Multiple tumors, indicated by the yellow arrows, exhibited high-density lesions throughout all lung regions. (C) Microscopic finding of lung metastasis lesion stained with hematoxylin-eosin. Scale bar, 500 μm.

Statistical analysis. All results were expressed as means (± standard deviations) without any notation. All statistical analyses were performed using Stata software ver.14.2 (Stata Corp., College Station, TX, USA). Statistical significance was set at P<0.05. Hierarchical clustering was performed using TAC software (Thermo Fisher Scientific), which utilizes the Euclidean distance metric and complete linkage method for clustering. The χ^2 test was performed to compare the original and pulmonary metastatic cells, and ANOVA followed by Bonferroni as a post hoc test were used for the other comparisons without any notation.

Table I. Comparison of lung metastasis rates between CMT93 and CMT93-PM1.

Cell line	Total mice, n	Mice with lung metastasis, n	Rate of lung metastasis, %	P-value
CMT93	15	2	13.3	P<0.001
CMT93-PM1	14	14	100.0	

Results

Evaluating the potential for lung metastasis of CMT93-PM cells and their original counterpart cells, CMT93. CMT93 is a commercially available cell line isolated from the rectum of a mouse with polypoid carcinoma and CMT93-PM1-4 are cell lines that we previously established from lung metastasis of CMT93 caused by tail vein injection (13). Initially, we confirmed the superior metastatic function of CMT93-PM1 compared with that of CMT93. CMT93-PM1 cells demonstrated a much more aggressive metastatic function than CMT93 cells using the tail vein injection method in 29 mice (Fig. 1). Visual inspection (Fig. 1A) and CT (Fig. 1B) revealed numerous metastatic tumors. We microscopically confirmed a metastatic lung lesion (Fig. 1C). Although the rate of lung metastasis was only 13.3% (2/15) in the CMT93 group, the CMT93-PM1 group showed a 100% metastasis rate (14/14) (P<0.001) (Table I).

Microarray, cluster analysis, and enrichment analysis by DAVID. We analyzed the gene expression profiles using microarray analysis to investigate the mechanisms underlying lung metastasis. We observed that 2241 and 88 genes showed differential expression CMT93 and CMT93-PM1 with a fold change of more than 2.0 and 10, respectively (Fig. 2). Among these 88 genes, 46 were upregulated and 42 were downregulated. The 88 genes were further divided into two groups using clustering analysis: genes that were upregulated or downregulated in CMT93-PM1 cells. The genes in these two groups were further subdivided into two groups. Cluster A (the most upregulated cluster in CMT93-PM1 cells compared to that in CMT93 cells) demonstrated phosphate metabolic processes, cell adhesion, cell proliferation, protein phosphorylation, and cellular metabolic processes. Cluster B (which included profilin 2) demonstrated upregulation of genes related to cell motility, adhesion, and migration. Clusters C and D consisted of genes that were downregulated in CMT93-PM1 cells compared to those in CMT93 cells. Cluster C contains several genes related to molecular transport. Cluster D contains genes related to hormone metabolism and regulation of cellular metabolic processes (Fig. 3A-D).

Evaluating PFN2 expression in CMT93-PM using RT-PCR and melting curve analysis. We focused on PFN2 because it showed the highest level of overexpression in CMT93-PM1 cells (Table SI). We confirmed the differential expression of PFN2 in the four cell lines of the CMT93-PM series using RT-PCR. The *PFN2* expression level was higher in CMT93-PM1-4 cells than in CMT93 cells, however we could not confirm a significant difference (Fig. 4A). These two PFN2 isoforms have distinct functions in malignancy (17).

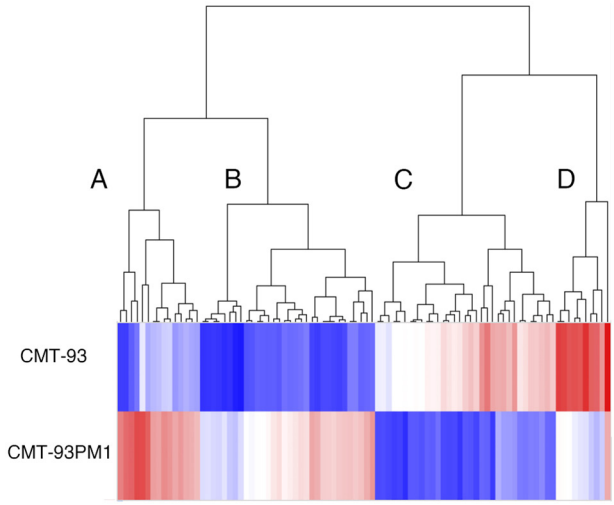

Figure 2. Comprehensive mRNA expression of CMT93 and CMT93-PM1 cells. The heat map illustrates the differential expression of 88 genes between CMT93-PM1 and CMT93 (absolute fold change ≥10). These 88 genes were classified into four groups (A, B, C, and D) using hierarchical clustering. Clusters A and B represent upregulated genes. Cluster A is the most upregulated in CMT93-PM1 cells compared with CMT93 cells, while cluster B shows a subordinate level of upregulation. Clusters C and D represent downregulated genes in CMT93-PM1 cells compared with CMT93 cells. Cluster D exhibits a more pronounced difference, while Cluster C shows a milder level of downregulation.

Two different melting temperatures suggested the presence of two different types of *PFN2* following melting curve analysis (Fig. 4B). PFN2A and PFN2B isoforms are splicing variants of *PFN2* with different distributions (18). The overall structure of PFN2 is illustrated in Fig. 5 (18,19). We confirmed that *PFN2A* showed significantly higher expression in CMT93-PM1-4 cell lines than in CMT93 cells (P<0.01) (Fig. 6A). As for PFN2B, we observed overexpression in CMT93-PM1-4 cell lines and a significant difference in CMT93-PM2 cells (P<0.01).

Discussion

The molecular mechanisms underlying lung metastasis in CRC have been extensively studied (8,9,12,13,20-23). However, the number of patients included in these studies was insufficient to obtain conclusive results owing to the heterogeneity of metastatic tumors (8,12,21). We can avoid the effects of tumor heterogeneity owing to varying patient backgrounds (such as a history of smoking, obesity, familial genomic problems, or other diseases, and previous treatments, such as chemotherapy and radiotherapy) using experimental animal models and cell lines. In a previous study, we injected mouse rectal cancer cells into the tail vein and observed lung metastases (13). We retrieved metastatic tumors and established their cell lines. To

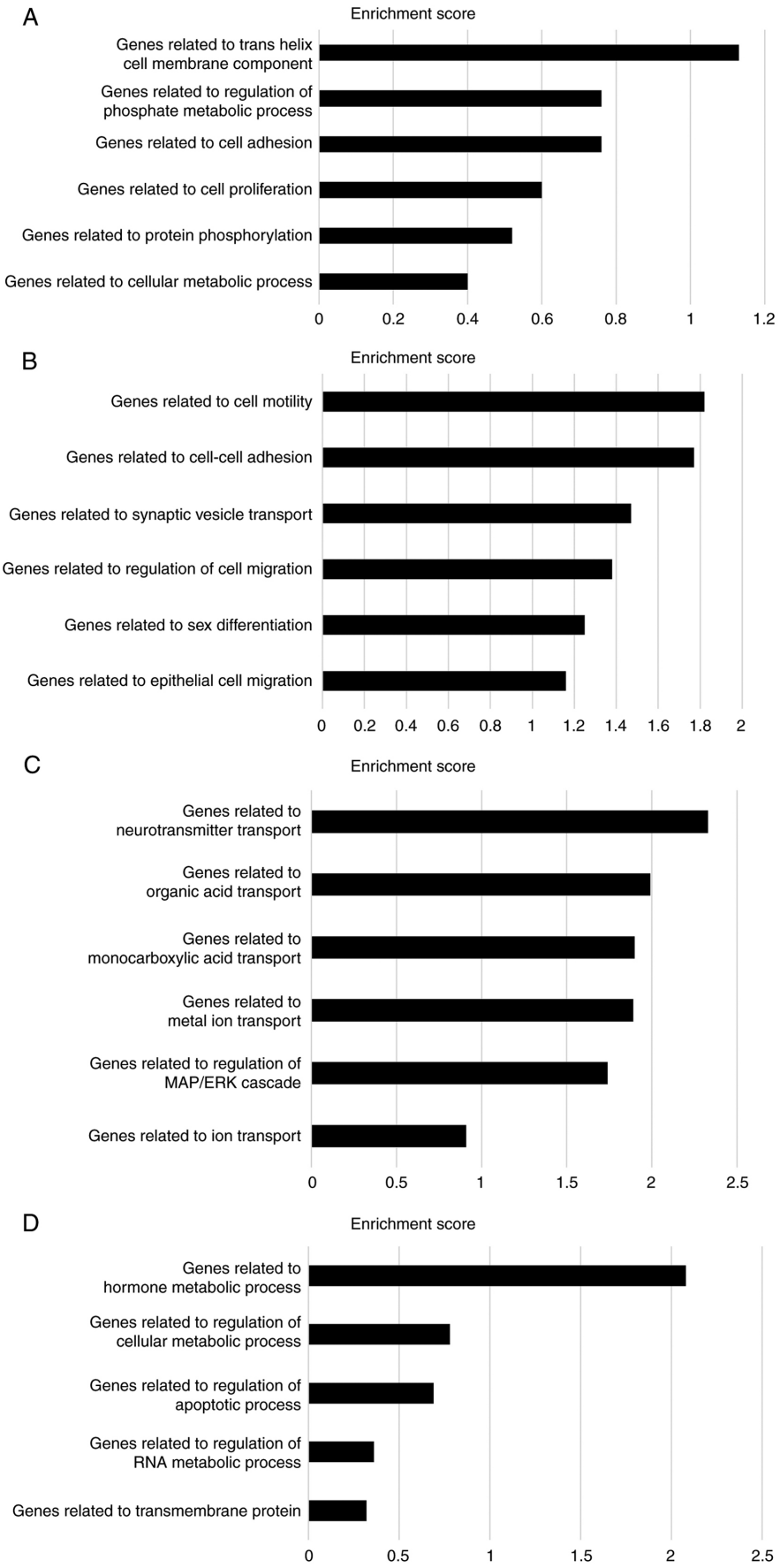

Figure 3. DAVID functional annotation clustering analysis of microarray data in CMT93-PM1 cells compared with that in the CMT93 cells. These bar charts illustrate the top six enhanced or reduced clusters in each cluster of CMT93-PM1 cells compared to those in CMT93 cells. (A) The most upregulated cluster in CMT93-PM1 cells compared with that in CMT93 cells. (B) The remaining upregulated clusters in CMT93-PM1 cells were higher compared with those in CMT93 cells. (C) Clusters Cconsisted of genes that are mildly downregulated in CMT93-PM1 cells compared to those in CMT93 cells. (D) The most downregulated cluster in CMT93-PM1 cells with that in CMT93 cells. DAVID, Database for Annotation, Visualization and Integrated Discovery.

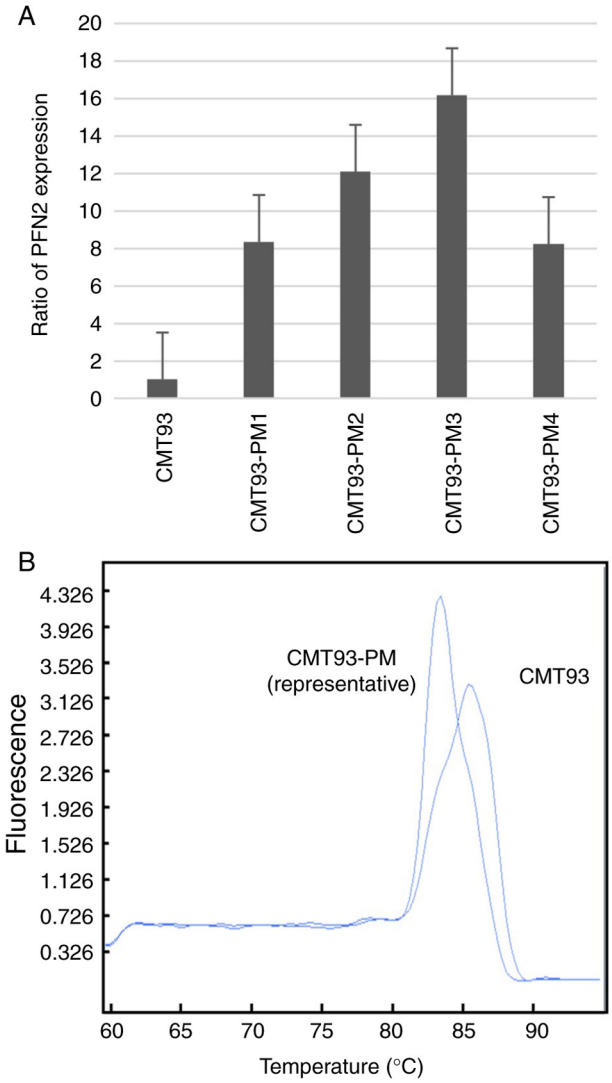

Figure 4. Evaluating *profilin2* expression and melting curve analysis. (A) RT-qPCR of PFN2 in CMT93-PM variant cell lines. A substantial increase in expression, ranging from approximately 5- to 10-fold, was observed across all cell lines. (B) High-resolution melting curve analysis of the RT-qPCR products of PFN2. This suggests the existence of two different peaks in a saddleback shape, implying the existence of splice variants of PFN2. PFN2, profilin 2; RT-qPCR, reverse transcription-quantitative PCR.

the best of our knowledge, this is the first cell line reported for the treatment of metastatic lung colorectal cancer. While three studies report the establishment or utilization of cell lines for liver metastases (24-26), none have focused on the establishment of cell lines for lung metastases. We found that the lung surfactant SP-D suppressed lung metastasis by inhibiting the epidermal growth factor receptor signaling using established cell lines. Our previous study suggests that environmental factors might affect lung metastasis in CRC (13). In this study, we conducted a global gene expression analysis to reveal the background of lung metastasis.

Initially, we confirmed the metastatic ability of CMT93-PM1 cells. Metastatic sites were formed by numerous homogeneous lesions in all the lungs. This form of lung metastasis differs from that observed in clinical situations because most human lung metastatic lesions form distinct nodules (27). However, this may be owing to the high clonality of the tumor cells, immune evasion specialized in the lung immune system, and the tail vein injection model. Multiple mechanisms can influence this phenomenon, including the upregulation of cell motility, cell adhesion, and invasion as well as the downregulation of tumor suppressor genes and the immune system. Therefore, we believe that employing technologies such as microarrays and investigating changes in a wide range of genomes are essential. This study provides new insights from this perspective.

Microarray analysis revealed that 88 genes were expressed with a fold change exceeding 10 times in CMT93-PM cells compared to that in CMT93 cells. Cluster analysis revealed four distinct clusters and subsequent enrichment analysis indicated that these clusters exhibited distinctive features. Clusters A and B consisting of genes upregulated in CMT93-PM1 cells were primarily associated with cell adhesion, proliferation, and motility. These functions are crucial for the formation of distant metastases, consistent with the results of previous studies (28-30). Notably, N-cadherin and VE-cadherin found within this cluster play significant roles in cell adhesion and migration and exhibit strong interactions with the wnt/β-catenin signaling pathway (31). The upregulation of N-cadherin expression in CRC tissues is negatively correlated with E-cadherin expression; furthermore, high N-cadherin expression promotes proliferation and migration of CRC cells by inducing EMT (32). *Six4* is another upregulated gene in cluster A and B that activates Akt and triggers the PI3K/Akt pathway (33). The PI3K/AKT/mammalian target of rapamycin signaling pathway is one of the most pivotal intracellular pathways, serving as a master regulator of cancer and enhancing cell growth and proliferation (34). Additionally, VCAM1 in this cluster promotes CRC invasion and metastasis by activating the EMT (35).

In contrast, clusters C and D comprised downregulated genes in CMT93-PM, and the roles of the genes in these clusters were markedly different from those in clusters A and B. Notably, a tumor suppressor gene [*tissue inhibitor of metalloproteinase-3* (*Timp3*)] was found in these clusters. TIMP3 plays various roles, one of which is the induction of apoptosis through caspase-dependent and-independent pathways (36). A decrease in *Timp3* expression correlates with the malignant behavior of colorectal cancer and TIMP3 overexpression results in reduced adhesion, migration, and invasion of human CRC cells *in vitro* (37). *PAX6* was detected in clusters C and D; it serves as a master control gene for the development of the eyes, other sensory organs, certain neural and epidermal tissues, and other homologous structures typically derived from ectodermal tissues. PAX6 is a potential tumor suppressor (38). Further investigations are required to assess the relationship between PAX6 and colorectal cancer and the several differences between CMT93 and CMT93-PM cells shown in this study.

We observed an overexpression of *PFN2* in the CMT93-PM series compared to that in the original CMT93 cells. Furthermore, *PFN2a* and *PFN2b* splicing variants were upregulated.

Profilins are actin-binding proteins that regulate cell structure by controlling signal-dependent actin polymerization (39). The *profilin* gene family comprises two major isoforms: *PFN1* and *PFN2* (40). Mouse *profilin I* is ubiquitously expressed in all

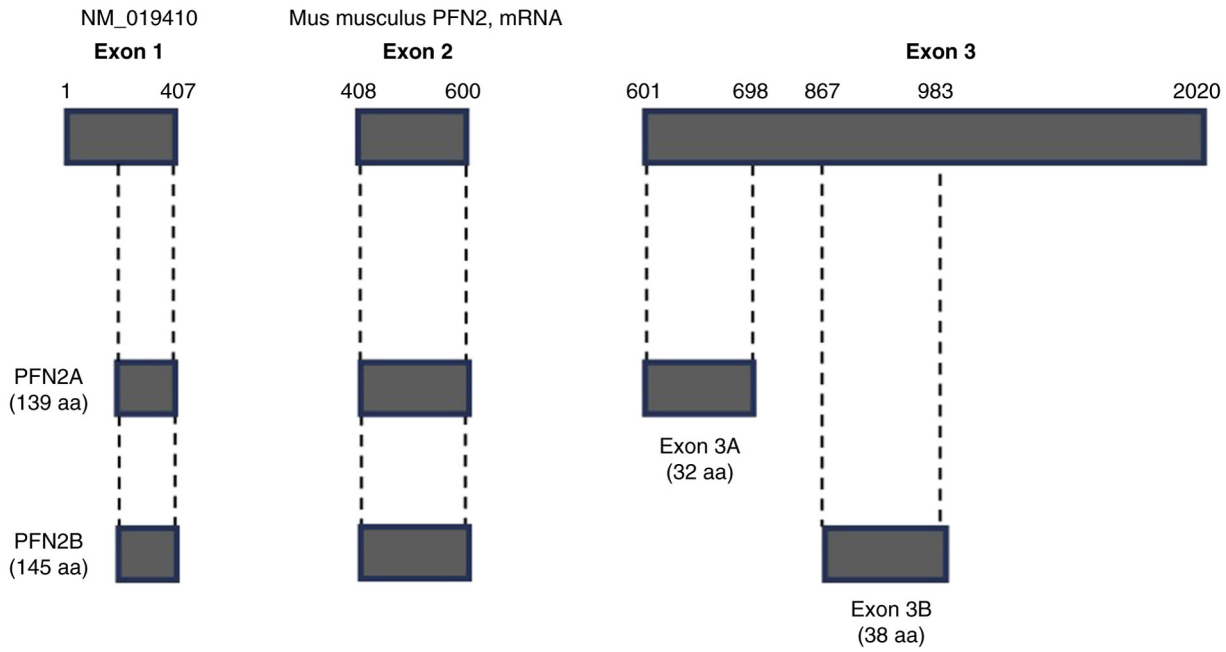

Figure 5. Molecular structure of profilin 2A and 2B. While both profiles share the same exons 1 and 2, the difference between the two is caused by two different types of exon 3 resulting from alternative splicing. PFN2, profilin 2.

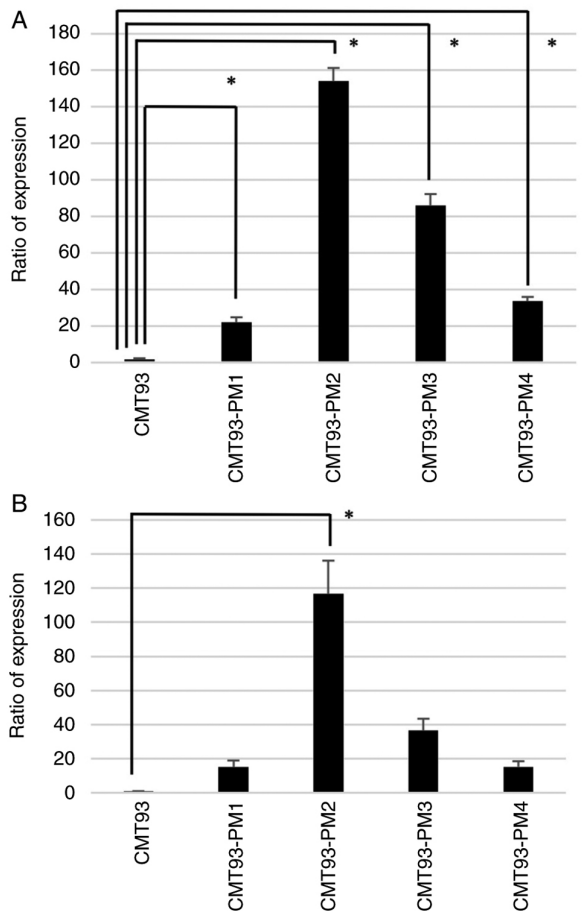

Figure 6. Expression of PFN2 splice forms confirmed by reverse transcription-quantitative PCR. (A) The levels of *PFN2A* in all the CMT93-PM variants. The expression levels of PFN2A were significantly higher in all CMT93-PM variants. (B) The levels of *PFN2B* in all the CMT93-PM variants. The expression levels of *PFN2B* were higher in all CMT93-PM variants. CMT93-PM2 cells exhibited a significant increase. *P<0.01. PFN2, profilin 2.

tissues except skeletal muscle, whereas *profilin IIA* is mainly expressed in neuronal tissues (41). Thus, *profilin I* appears to be a housekeeping gene that is important for vital functions, whereas *profilin II* was later developed to serve specific functions, mainly in the brain. PFN2 is alternately spliced into PFN2a and 2b. Among these, PFN2a is the predominant splice form (18,19) that is conserved across vertebrates, including humans, mice, chickens, and cattle. Research on the functions of PFN2a has primarily focused on cell migration and the mammalian nervous system, including synaptic vesicle exocytosis and neuronal excitability (42). The relationship between PFN2 and lung, breast, and prostate cancers was previously investigated (17,39,43,44). PFN2 regulates growth by inhibiting nuclear localization of histone deacetylase 1 (HDAC1) in lung cancer (43). It promotes the progression of small cell lung cancer *in vitro* and *in vivo* and regulates angiogenesis in the tumor microenvironment through cancer-derived exosomes (45).

Only two reports have described the role of PFN2 in colorectal cancer and no previous study has described the relationship between PFN2 isoforms and colorectal cancer. PFN2 promotes the metastatic potential and stemness of colorectal CSCs by regulating EMT- and stemness-related proteins (45). These findings were consistent with our results. In contrast, the loss of *PFN2* contributes to enhanced epithelial-mesenchymal transition and metastasis (46). Their observations are inconsistent with our results, since they concluded that the loss of *PFN2* exacerbates metastasis, leading them to insist that PFN2 inhibits tumor metastasis. However, their study has several limitations. First, although they concluded that PFN2 downregulation enhanced cell migration, they compared two different cell lines: SW620 and HCT116. Different cell lines have distinct genetic backgrounds in addition to *PFN2* expression. Therefore, comparisons between different cell lines are not particularly informative. Second, a retrovirus

was used to transfect *PFN2* into SW620 cells. However, the retroviral vector method does not offer precise control over the location of transfection and is often associated with the activation of tumor-related genes. Third, *in vitro* experiments were conducted, and the results were validated *in vivo*. These factors could have contributed to the potential differences between the results of their study and ours.

Our study has some limitations. First, we used a single cell line (CMT93) as a model. Therefore, it is essential to examine multiple cell lines to validate our results. Secondly, we used the tail vein injection method with CMT93-PM and confirmed a significant difference in metastatic function between CMT93-PM and CMT93. However, the tail vein injection method has positive and negative aspects for evaluating lung metastasis. In this method, metastasis is initiated via tail vein injection, which mimics the natural progression of colorectal cancer. After injection, tumor cells were disseminated swiftly through systemic venous perfusion. However, our experiment did not recapitulate metastasis in these patients because the tumor cells were dispersed by proteinase before injection. Thirdly, we used the cells derived from the metastatic tumors in lungs, and the similarity of the established cell lines with the original tumors, and the homogeneity of the cells from the metastatic lesions were not be verified. Fourth, our experiments are solely based on RNA and cDNA, lacking evidence of protein expression levels for the two different types of PFN2. This was due to the unavailability of the corresponding antibodies commercially. Finally, we did not study the effects of *PFN2* overexpression on cell behavior. Further investigations into the function of PFN2 and the relationship between lung metastasis and PFN2 are necessary to validate the clinical utility of our findings. This validation may be achieved using pathological materials and publicly available datasets. Additionally, the role of each variant remains unclear. Studies on PFN2a and PFN2b will provide deeper insights into the molecular mechanisms of lung metastasis in CRC.

We established an *in vitro* lung metastasis model using colorectal cancer cells and mice. Differential gene expression analysis was used to identify genes associated with lung metastasis. Thus, our model provides a unique platform to study lung metastasis. The functional significance and clinical utility of these two PFN2 isoforms should be considered in future studies.

Acknowledgements

The authors would like to thank Ms. Kaoru Hattori (Department of Surgery, Keio University School of Medicine, Tokyo, Japan) for their technical support and handling of the mice, Dr. Shingo Akimoto (Department of Surgery, Keio University School of Medicine, Tokyo, Japan) for their support during this study, and Dr. Shinya Saito (Oncogene Research Unit/Cancer Prevention Unit, Tochigi Cancer Center Research Institute, Utsunomiya, Japan) for providing insightful instructions and support during the experiments.

Funding

No funding was received.

Availability of data and materials

The datasets generated and analyzed in the current study are available from the GEO repository (https://www.ncbi.nlm.nih.gov/geo/query/acc.cgi?acc=GSE252603). GEO accession number is GSE252603. The rest of the data generated in the present study may be requested from the corresponding author.

Authors' contributions

NT and MT participated in the study design, coordination, and drafting of manuscript. YT and YY performed the experiments and acquired data. KS and KO participated in the study design and performed statistical analyses. MT and TK confirm the authenticity of all the raw data. HH, SF, TK, IO, and YK conceived the study, participated in its design and coordination, and helped draft the manuscript. All authors have read and approved the final manuscript and agree to be accountable for all aspects of the study.

Ethics approval and consent to participate

All procedures were performed with the approval of the Laboratory Animal Care and Use Committee at the Keio University School of Medicine (approval no. 15006).

Patient consent for publication

Not applicable.

Competing interests

The authors declare that they have no competing interests.

References

1. Keum N and Giovannucci E: Global burden of colorectal cancer: Emerging trends, risk factors and prevention strategies. Nat Rev Gastroenterol Hepatol 16: 713-732, 2019.
2. Van Cutsem E, Cervantes A, Adam R, Sobrero A, Van Krieken JH, Aderka D, Aguilar EA, Bardelli A, Benson A, Bodoky G, *et al*: ESMO consensus guidelines for the management of patients with metastatic colorectal cancer. Ann Oncol 27: 1386-1422, 2016.
3. Muratore A, Zorzi D, Bouzari H, Amisano M, Massucco P, Sperti E and Capussotti L: Asymptomatic colorectal cancer with un-resectable liver metastases: Immediate colorectal resection or up-front systemic chemotherapy? Ann Surg Oncol 14: 766-770, 2007.
4. Van Cutsem E, Nordlinger B, Adam R, Köhne CH, Pozzo C, Poston G, Ychou M and Rougier P; European Colorectal Metastases Treatment Group: Towards a pan-European consensus on the treatment of patients with colorectal liver metastases. Eur J Cancer 42: 2212-2221, 2006.
5. Parnaby CN, Bailey W, Balasingam A, Beckert L, Eglinton T, Fife J, Frizelle FA, Jeffery M and Watson AJ: Pulmonary staging in colorectal cancer: A review. Colorectal Dis 14: 660-670, 2012.
6. Watanabe T, Muro K, Ajioka Y, Hashiguchi Y, Ito Y, Saito Y, Hamaguchi T, Ishida H, Ishiguro M, Ishihara S, *et al*: Japanese society for cancer of the colon and rectum (JSCCR) guidelines 2016 for the treatment of colorectal cancer. Int J Clin Oncol 23: 1-34, 2018.
7. Chandra R, Karalis JD, Liu C, Murimwa GZ, Voth Park J, Heid CA, Reznik SI, Huang E, Minna JD and Brekken RA: The colorectal cancer tumor microenvironment and its impact on liver and lung metastasis. Cancers (Basel) 13: 6206, 2021.
8. Zhang N, Di J, Wang Z, Gao P, Jiang B and Su X: Genomic profiling of colorectal cancer with isolated lung metastasis. Cancer Cell Int 20: 281, 2020.

9. Yamamoto T, Kawada K, Itatani Y, Inamoto S, Okamura R, Iwamoto M, Miyamoto E, Chen-Yoshikawa TF, Hirai H, Hasegawa S, *et al*: Loss of SMAD4 promotes lung metastasis of colorectal cancer by accumulation of CCR1+ tumor-associated neutrophils through CCL15-CCR1 axis. Clin Cancer Res 23: 833-844, 2017.
10. Liu J, Shao Y, He Y, Ning K, Cui X, Liu F, Wang Z and Li F: MORC2 promotes development of an aggressive colorectal cancer phenotype through inhibition of NDRG1. Cancer Sci 110: 135-146, 2019.
11. Hu XT, Xing W, Zhao RS, Tan Y, Wu XF, Ao LQ, Li Z, Yao MW, Yuan M, Guo W, *et al*: HDAC2 inhibits EMT-mediated cancer metastasis by downregulating the long noncoding RNA H19 in colorectal cancer. J Exp Clin Cancer Res 39: 270, 2020.
12. Kim SH, Choi SJ, Cho YB, Kang MW, Lee J, Lee WY, Chun HK, Choi YS, Kim HK, Han J and Kim J: Differential gene expression during colon-to-lung metastasis. Oncol Rep 25: 629-636, 2011.
13. Tajima Y, Tsuruta M, Hasegawa H, Okabayashi K, Ishida T, Yahagi M, Makino A, Koishikawa K, Akimoto S, Sin DD and Kitagawa Y: Association of surfactant protein D with pulmonary metastases from colon cancer. Oncol Lett 20: 322, 2020.
14. Huang DW, Sherman BT, Tan Q, Kir J, Liu D, Bryant D, Guo Y, Stephens R, Baseler MW, Lane HC and Lempicki RA: David bioinformatics resources: Expanded annotation database and novel algorithms to better extract biology from large gene lists. Nucleic Acids Res 35: W169-W175, 2007.
15. Huang R, Yuan DJ, Li S, Liang XS, Gao Y, Lan XY, Qin HM, Ma YF, Xu GY, Schachner M, *et al*: NCAM regulates temporal specification of neural progenitor cells via profilin2 during corticogenesis. J Cell Biol 219: e201902164, 2020
16. Livak KJ and Schmittgen TD: Analysis of relative gene expression data using real-time quantitative PCR and the 2(-Delta Delta C(T)) method. Methods 25: 402-408, 2001.
17. Mouneimne G, Hansen SD, Selfors LM, Petrak L, Hickey MM, Gallegos LL, Simpson KJ, Lim J, Gertler FB, Hartwig JH, *et al*: Differential remodeling of actin cytoskeleton architecture by profilin isoforms leads to distinct effects on cell migration and invasion. Cancer Cell 22: 615-630, 2012.
18. Lambrechts A, Braun A, Jonckheere V, Aszodi A, Lanier LM, Robbens J, Van Colen I, Vandekerckhove J, Fässler R and Ampe C: Profilin II is alternatively spliced, resulting in profilin isoforms that are differentially expressed and have distinct biochemical properties. Mol Cell Biol 20: 8209-8219, 2000.
19. Di Nardo A, Gareus R, Kwiatkowski D and Witke W: Alternative splicing of the mouse profilin II gene generates functionally different profilin isoforms. J Cell Sci 113: 3795-3803, 2000.
20. Wang H, Fu W, Im JH, Zhou Z, Santoro SA, Iyer V, DiPersio CM, Yu QC, Quaranta V, Al-Mehdi A and Muschel RJ: Tumor cell alpha3beta1 integrin and vascular laminin-5 mediate pulmonary arrest and metastasis. J Cell Biol 164: 935-941, 2004.
21. Shu R, Xu Y, Tian Y, Zeng Y, Sun L, Gong F, Lei Y, Wang K and Luo H: Differential expression profiles of long noncoding RNA and mRNA in colorectal cancer tissues from patients with lung metastasis. Mol Med Rep 17: 5666-5675, 2018.
22. Tang L, Lei YY, Liu YJ, Tang B and Yang SM: The expression of seven key genes can predict distant metastasis of colorectal cancer to the liver or lung. J Dig Dis 21: 639-649, 2020.
23. Dai W, Guo C, Wang Y, Li Y, Xie R, Wu J, Yao B, Xie D, He L, Li Y, *et al*: Identification of hub genes and pathways in lung metastatic colorectal cancer. BMC Cancer 23: 323, 2023.
24. Lu M, Zessin AS, Glover W and Hsu DS: Activation of the mTOR pathway by oxaliplatin in the treatment of colorectal cancer liver metastasis. PLoS One 12: e0169439, 2017.
25. Li LN, Zhang HD, Yuan SJ, Tian ZY and Sun ZX: Establishment and characterization of a novel human colorectal cancer cell line (CLY) metastasizing spontaneously to the liver in nude mice. Oncol Rep 17: 835-840, 2007.
26. Govaert KM, Emmink BL, Nijkamp MW, Cheung ZJ, Steller EJ, Fatrai S, de Bruijn MT, Kranenburg O and Rinkes IH: Hypoxia after liver surgery imposes an aggressive cancer stem cell phenotype on residual tumor cells. Ann Surg 259: 750-759, 2014.
27. Salah S, Ardissone F, Gonzalez M, Gervaz P, Riquet M, Watanabe K, Zabaleta J, Al-Rimawi D, Toubasi S, Massad E, *et al*: Pulmonary metastasectomy in colorectal cancer patients with previously resected liver metastasis: Pooled analysis. Ann Surg Oncol 22: 1844-1850, 2015.
28. Wang JY, Sun J, Huang MY, Wang YS, Hou MF, Sun Y, He H, Krishna N, Chiu SJ, Lin S, *et al*: STIM1 overexpression promotes colorectal cancer progression, cell motility and COX-2 expression. Oncogene 34: 4358-4367, 2015.
29. Jackstadt R, Röh S, Neumann J, Jung P, Hoffmann R, Horst D, Berens C, Bornkamm GW, Kirchner T, Menssen A and Hermeking H: AP4 is a mediator of epithelial-mesenchymal transition and metastasis in colorectal cancer. J Exp Med 210: 1331-1350, 2013.
30. Eckey M, Kuphal S, Straub T, Rümmele P, Kremmer E, Bosserhoff AK and Becker PB: Nucleosome remodeler SNF2L suppresses cell proliferation and migration and attenuates Wnt signaling. Mol Cell Biol 32: 2359-2371, 2012.
31. Katoh M: Multi-layered prevention and treatment of chronic inflammation, organ fibrosis and cancer associated with canonical WNT/β-catenin signaling activation (Review). Int J Mol Med 42: 713-725, 2018.
32. Yan X, Yan L, Liu S, Shan Z, Tian Y and Jin Z: N-cadherin, a novel prognostic biomarker, drives malignant progression of colorectal cancer. Mol Med Rep 12: 2999-3006, 2015.
33. Sun X, Hu F, Hou Z, Chen Q, Lan J, Luo X, Wang G, Hu J and Cao Z: SIX4 activates Akt and promotes tumor angiogenesis. Exp Cell Res 383: 111495, 2019.
34. Yang J, Nie J, Ma X, Wei Y, Peng Y and Wei X: Targeting PI3K in cancer: Mechanisms and advances in clinical trials. Mol Cancer 18: 26, 2019.
35. Zhang D, Bi J, Liang Q, Wang S, Zhang L, Han F, Li S, Qiu B, Fan X, Chen W, *et al*: VCAM1 promotes tumor cell invasion and metastasis by inducing EMT and transendothelial migration in colorectal cancer. Front Oncol 10: 1066, 2020.
36. Kallio JP, Hopkins-Donaldson S, Baker AH and Kähäri VM: TIMP-3 promotes apoptosis in nonadherent small cell lung carcinoma cells lacking functional death receptor pathway. Int J Cancer 128: 991-996, 2011.
37. Lin H, Zhang Y, Wang H, Xu D, Meng X, Shao Y, Lin C, Ye Y, Qian H and Wang S: Tissue inhibitor of metalloproteinases-3 transfer suppresses malignant behaviors of colorectal cancer cells. Cancer Gene Ther 19: 845-851, 2012.
38. Kiselev Y, Andersen S, Johannessen C, Fjukstad B, Olsen KS, Stenvold H, Al-Saad S, Donnem T, Richardsen E, Bremnes RM and Busund LT: Transcription factor PAX6 as a novel prognostic factor and putative tumour suppressor in non-small cell lung cancer. Sci Rep 8: 5059, 2018.
39. Ma CY, Zhang CP, Zhong LP, Pan HY, Chen WT, Wang LZ, Andrew OW, Ji T and Han W: Decreased expression of profilin 2 in oral squamous cell carcinoma and its clinicopathological implications. Oncol Rep 26: 813-823, 2011.
40. Jeong DH, Choi YN, Seo TW, Lee JS and Yoo SJ: Ubiquitin-proteasome dependent regulation of Profilin2 (Pfn2) by a cellular inhibitor of apoptotic protein 1 (cIAP1). Biochem Biophys Res Commun 506: 423-428, 2018.
41. Witke W, Podtelejnikov AV, Di Nardo A, Sutherland JD, Gurniak CB, Dotti C and Mann M: In mouse brain profilin I and profilin II associate with regulators of the endocytic pathway and actin assembly. EMBO J 17: 967-976, 1998.
42. Boyl PP, Di Nardo A, Mulle C, Sassoè-Pognetto M, Panzanelli P, Mele A, Kneussel M, Costantini V, Perlas E, Massimi M, *et al*: Profilin2 contributes to synaptic vesicle exocytosis, neuronal excitability, and novelty-seeking behavior. EMBO J 26: 2991-3002, 2007.
43. Tang YN, Ding WQ, Guo XJ, Yuan XW, Wang DM and Song JG: Epigenetic regulation of Smad2 and Smad3 by profilin-2 promotes lung cancer growth and metastasis. Nat Commun 6: 8230, 2015.
44. Obinata D, Funakoshi D, Takayama K, Hara M, Niranjan B, Teng L, Lawrence MG, Taylor RA, Risbridger GP, Suzuki Y, *et al*: OCT1-target neural gene PFN2 promotes tumor growth in androgen receptor-negative prostate cancer. Sci Rep 12: 6094, 2022.
45. Cao Q, Liu Y, Wu Y, Hu C, Sun L, Wang J, Li C, Guo M, Liu X, Lv J, *et al*: Profilin 2 promotes growth, metastasis, and angiogenesis of small cell lung cancer through cancer-derived exosomes. Aging (Albany NY) 12: 25981-25999, 2020.
46. Zhang H, Yang W, Yan J, Zhou K, Wan B, Shi P, Chen Y, He S and Li D: Loss of profilin 2 contributes to enhanced epithelial-mesenchymal transition and metastasis of colorectal cancer. Int J Oncol 53: 1118-1128, 2018.